Simulation-based study of the influence of particle physical properties on fertilizer spreading ability

Tien-Thinh Le, Emmanuel Piron, Denis Miclet, Sylvain Villette

Computers and Electronics in Agriculture 229 (2025) 109753

Contents lists available at ScienceDirect

Computers and Electronics in Agriculture

journal homepage: www.elsevier.com/locate/compag

Simulation-based study of the influence of particle physical properties on fertilizer spreading ability

Tien-Thinh Le [a], Emmanuel Piron [a], Denis Miclet [a], Sylvain Villette [a,b,*]

[a] Université Clermont Auvergne, INRAE, UR TSCF, AgroTechnoPôle, Domaine des Palaquins, 40 route de Chazeuil, F-03150 Montoldre, France
[b] Institut Agro, 26 bd Docteur Petitjean, F-21000 Dijon, France

ARTICLE INFO

Keywords:
Particle size distribution
Drag coefficient
Density
Throw distance
Working width
Spread pattern

ABSTRACT

Despite spreader performance, different fertilizers are known to have inherent limitations that prevent them from achieving the same working width at a targeted spreading quality. Nevertheless, there is currently no mathematical relationship to express the maximum working width achievable by a fertilizer as a function of its physical properties. The aim of this paper is to develop a numerical method to provide such a mathematical relationship. Since the maximum working width W_{WCV10} ensuring a satisfying uniformity (CV≤10%) is a complex parameter (resulting from different stages of the spreading process), the issue has been decomposed into two steps. First, a dataset is computed by numerical simulations. 3800 virtual fertilizers are designed and feed into numerical simulations based on a Monte Carlo process. For each fertilizer, twin disk spread patterns are computed for a set of virtual spreader settings. Then, W_{WCV10} is deduced from simulations of adjacent passes and overlaps. The mean radius R_m of the spread pattern is also computed. Second, based on this consistent dataset, multivariate polynomial regressions are established to express W_{WCV10} and R_m as mathematical functions of 5 independent physical characteristics of the fertilizer: the drag coefficient, the specific density and three particle size distribution parameters. Thus, for the first time, the contribution of each variable (to the ability of the fertilizer to achieve a working width) is quantified and the sensitivity of W_{WCV10} and R_m is analyzed by using partial derivatives. The correlation between W_{WCV10} and R_m is also demonstrated.

1. Introduction

Spreading uniformity directly affects the efficiency and environmental impact of fertilizers (Gyldengren et al., 2020; Miller et al., 2009; Richards and Hobson, 2013; Tissot et al., 2002). To achieve maximum work output, farmers aim to utilize the largest possible working width (*i.e.* distance between successive tractor tracks) while maintaining an acceptable level of application uniformity. This uniformity is typically evaluated calculating the coefficient of variation (CV) of adjacent, overlapping transverse distributions and a CV less than 15 % indicates correct application (EN 13739–2, 2011).

For applying granular fertilizers, centrifugal spreaders are the primary method across Europe. This process consists of two main stages: the motion of the particles on a spinning disk and the ballistic flight of the particles.

Concerning the first stage, the characteristics of the disk influence the motion of the particles on its vanes, and ultimately affect the particle ejection. Numerous works studied on-disk motion and expressed outlet parameters as functions of the disk geometry and revolution speed using analytical approaches (Hofstee, 1995; Olieslagers, 1997; Villette et al., 2005). Experimental works also studied the influence of disk characteristics such as vane shape and profile (Fulton et al., 2020; Yildirim, 2008), cone angle (Yildirim, 2006) or revolution speed (Villette et al., 2012; Yildirim, 2006). These works demonstrated that target ejection characteristics (velocity and mass flow distribution around the disk) can be achieved by designing appropriate spreader hardware components. Thus, although particle ejection results from interactions between the particles and the spinning disk, it has been established that the particle ejection characteristics can be controlled by designing suitable parts and adjusting mechanical parameters of the spreader. These ejection characteristics, controlled by the spreader, are the initial parameters of the fertilizer ballistic flight.

On the opposite, once the particles left the spinning disk, the second stage of motion (*i.e.* ballistic flight) does not depend on spreader

* Corresponding author at: Université Clermont Auvergne, INRAE, UR TSCF, AgroTechnoPôle, Domaine des Palaquins, 40 route de Chazeuil, F-03150 Montoldre, France.
E-mail address: sylvain.villette@institut-agro.fr (S. Villette).

https://doi.org/10.1016/j.compag.2024.109753
Received 7 May 2024; Received in revised form 27 November 2024; Accepted 30 November 2024
Available online 12 December 2024

performances. It only depends on fertilizer physical properties. Size, specific density and drag coefficient have been known to be properties that affect the motion of fertilizer particles through the air (Hofstee and Huisman, 1990). Historically, the effects of these properties have mainly been studied in the context of preventing ballistic segregation during blended fertilizer spreading. Most experimental studies have highlighted segregation issues (Hoffmeister et al., 1964; Thaper et al., 2021; Virk et al., 2013; Yule, 2011), particularly due to size variability between fertilizer components, but they have not established any mathematical relationship between physical properties and spreading performance indicators. Miserque et al. (2008) were the only authors to mathematically related fertilizer physical characteristics to a ground distribution characteristic. They related the particle properties to the spreading width, which is the distance between the extreme left and right points where the fertilizer lands on the ground. Thus, they developed a multivariate regression model ($R^2 = 0.60$) to predict spreading width as a function of particle median diameter of the blend and density of the heaviest component. This study has interestingly highlighted the impact of particle characteristics on their ability to be projected up to a given distance. However, it focused on fertilizer mixtures and the risk of segregation between the components of the mixture.

Studying the influence of fertilizer physical properties is challenging through experimental measurements due to two main difficulties: first, separating the spreading process into on-disk and off-disk steps and second, isolating the impact of individual properties. Another way is to study the impact of fertilizer characteristics using theoretical models to compute particle ballistic flights. Using approximating equations for ballistic trajectories, Pitt et al. (1982) studied the influence of particle size variability on the variability in throw distance for a given initial velocity and height. They concluded that variation in particle size has only a mild effect on the lateral distribution of particles. They also modelled the transverse spread pattern assuming simple uniform distributions of particle drop point onto the spinning disk and derived U-shaped transverse spread patterns. Nevertheless, the effect of particle size distribution on the transverse spread pattern were not studied and adjacent overlaps were not considered. Based on the study of transverse spread patterns for granulated urea, prilled urea, and ammonium nitrate, Parkin et al. (2005) suggested calculating the theoretical stop distance as a characteristic parameter to compare the ability of fertilizers to reach the same spreading width. Nevertheless, this approach has not been explored in subsequent studies. Antille et al. (2013) suggested the particle size range of new fertilizers could be designed to meet a target working width and proposed to compute the ballistic flight to assess whether particle physical properties suited the spreading objective. The model predicted the throw distance of individual particles but did not simulate the spread pattern and did not address the working width. Grafton et al. (2015) also proposed using a ballistic model to investigate how fertilizer characteristics influence working width. The authors compared working widths deduced from experimental measurements with throw distances computed for fertilizer mean particle size but no mathematical relationship has been established.

Thus, no general relationship has ever been established in literature between the maximum achievable working width and other spreading characteristics such as the mean radius of the spread pattern. Furthermore, no mathematical relationship has ever been established between the fertilizer physical properties and the maximum working width. Consequently, there is a lack of models that can evaluate and compare fertilizers based on their ability to achieve a target working width with uniform distribution. Additionally, no model makes it possible to evaluate the respective contribution of the different physical properties. In practice, this leads fertilizer producers to still wonder about which product properties to modify to improve fertilizer spreading ability.

The objective of the study is to fill these gaps by demonstrating that the maximum achievable working width is linearly related to the spread pattern mean radius, and by expressing theses spreading parameters as functions of fertilizer physical properties. The maximum working width

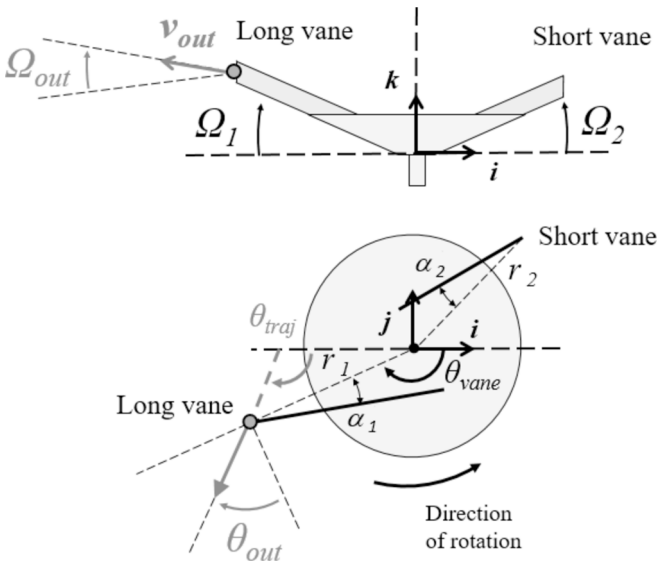

Fig. 1. Side view (top) and top view (bottom) of the counterclockwise S8 disk: r_1, α_1, Ω_1 are the radius, pitch angle and vertical angle respectively for the long vane and r_2, α_2, Ω_2 for the short vane; $\boldsymbol{v_{out}}$, θ_{out}, and Ω_{out} are the outlet velocity vector, the horizontal outlet angle and vertical outlet angle respectively; θ_{traj} is the horizontal angle of the trajectory; θ_{vane} is the angular location of the vane; $\boldsymbol{i}$, $\boldsymbol{j}$, $\boldsymbol{k}$, vectors of a right handed Cartesian coordinate system centered on the disk axle. The particle ejection is illustrated when a particle leaves the long vane.

is a complex parameter, influenced by particle ballistic behavior, spreader adjustment and pass overlap. Consequently, the experimental study of the maximum working width as a function of fertilizer characteristics is unrealistic, while the theoretical study is impossible by classical mechanical approaches. The originality of this study consists in using numerical simulations to compute the working widths and the corresponding CVs for a large number of virtual fertilizers in order to obtain a database, which then feeds a regression analysis to establish the mathematical relationships relating the maximum working width to the physical characteristics of the fertilizer.

The study has four main contributions:

i) the development of a numerical method to provide a consistent set of maximum working width values computed for a wide range of fertilizer physical properties;
ii) the establishment of a mathematical model relating the maximum working width and the spread pattern mean radius to five independent variables describing fertilizer physical properties;
iii) the analysis of the relative contribution of each physical property on the ability of the fertilizer to achieve a targeted working width;
iv) the demonstration of the correlation between the maximum working width and the mean radius of the corresponding spread pattern.

2. Materials and methods

In this study, the fertilizer spreading ability was studied by computing two spreading performance indicators: the maximum working width W_{WCV10} ensuring a satisfying uniformity (CV≤10%) and the mean radius R_m of the spread pattern. To isolate the impact of the physical properties of fertilizers on these two indicators, independently of spreader characteristics, the study assumed the same initial conditions of ballistic flight for all fertilizers and only simulated the second stage of the spreading process: from the disk ejection to the particle distribution on the ground after adjacent overlaps.

Table 1
Characteristics of the S8 disk.

Parameters	Nomenclature	Long vane ($i = 1$)	Short vane ($i = 2$)
Vane characteristic			
Radius of the vane	r_i	415	375
Pitch angle of the vane	α_i	5.4°	9.7°
Vertical angle of the vane	Ω_i	9.8°	8.8°
Mass flow proportion	p	43 %	57 %
Revolution speed	ω	900 rpm	
Disk spacing*	d_D	1.4 m	

* distance between the axle of the right and left disks on the spreader AXIS 50.1.

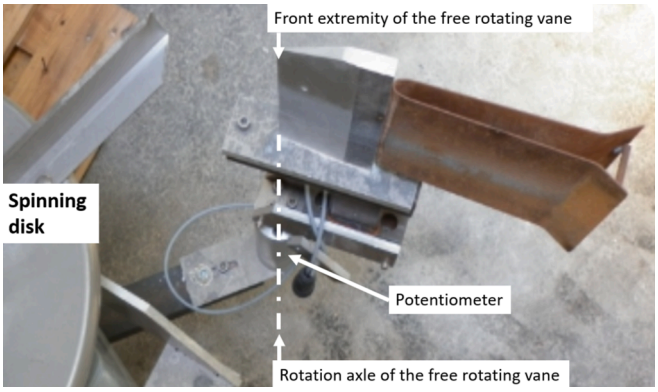

Fig. 2. Free rotating wind vane used to measure the horizontal outlet angle.

The measurement devices used to provide experimental data are presented in section 2.1. The characteristics of the actual and virtual fertilizers used for experimental and simulated data are presented in section 2.2. Models and simulations developed to compute R_m and W_{WCV10} are described in section 2.3. The regression model developed to R_m and W_{WCV10} as function of the fertilizer properties is described in section 2.4. Obtaining experimental values for R_m and W_{WCV10} is explained in section 2.5.

2.1. Experimental devices

2.1.1. Spinning disks

In this study, simulation results were compared to experimental data obtained with a marketed spinning disk, which was the S8 disk, commonly used with AXIS 50.1 spreaders supplied by RAUCH Company (Germany). This was a concave disk equipped with two straight pitched vanes of two different lengths. The revolution speed was 900 rpm. Fig. 1 presents the design of the counterclockwise disk. Table 1 provides the parameter values. The proportion p of the mass flow collected by each vane was deduced from the angular location of the vanes on the disk.

For specific needs of certain stages of the study (described in following sections), three other custom-made counterclokwise disks had also been punctually used. The first one, called S8L had the same characteristics than the S8 disk except that it is equipped with two long vanes. The second one, called S8S had the same characteristics than the S8 disk except that it is equipped with two short vanes. The last one, called SD was a simplified concave disk equipped with two radial vanes with the following characteristics: the radius was 395 mm and the vertical angle of the vanes was 13.5°.

2.1.2. Horizontal outlet angle measurement

The horizontal outlet angle θ_{out} (Fig. 1) of the particles (when they leave the vane) was measured using a free rotating wind vane forced in direction by the particle flow movement (Fig. 2). This measurement principle has already been used by (Heppler, 1993; Persson, 1996). The narrow extremity of the wind vane was fixed to the upper end of a rotation shaft mounted on ball bearings. A single-turn rotary potentiometer was mounted at the lower end of the shaft and was used to provide an analog signal from 0 to 10 V linearly related to the rotation angle (0 to 360°). The analog signal was sampled and recorded with a frequency of 10 Hz. Previous to measurements, a geometrical setting was carried out so that the value was 90° when the vane axis is aligned with the radius of the spinning disk and is 0° when the vane axis is orthogonal to the radius of the disk. Since the rotation axle of the free vane cannot be placed just on the outer radius of the centrifugal disk, a geometrical correction was established to convert the angle value measured in the vicinity of the disk into the angle value at the disk edge. The mean value $\mu\theta_{out}$ and the standard deviation $\sigma\theta_{out}$ of the horizontal outlet angle were deduced from 15 successive measurements.

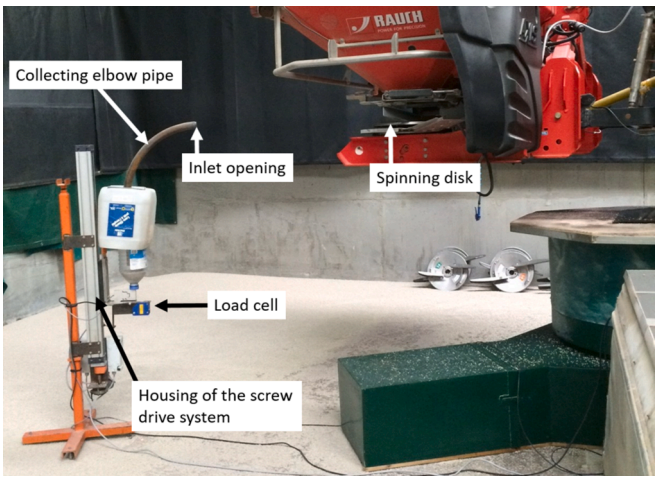

Fig. 3. Collecting elbow pipe used to measure the vertical outlet angle.

2.1.3. Vertical outlet angle measurement

The vertical outlet angle Ω_{out} (Fig. 1) of the particles (when they leave the vane) was measured using a collecting elbow pipe with inlet opening placed in front of the spinning disk and with outlet opening feeding a container mounted on load cell (Fig. 3). The inlet opening was 36 mm in diameter. The vertical motion of the collecting device was obtained by means of an electrical motor and a rotating screw. The rotation of the screw was transformed into linear motion of a movable nut on which is fixed the collecting device. The vertical motion of the device was controlled at 2 mm/s. The vertical location was measured with a laser telemeter. During the motion of the elbow pipe, the vertical location of the opening and the particle collected weight were simultaneously recorded (with a frequency of 5 Hz). This provide the vertical distribution of the mass flow at the measurement location. The mean value $\mu\Omega_{out}$ and the standard deviation $\sigma\Omega_{out}$ of the vertical outlet angle were deduced from the measured distribution compared to the vertical location of the outer vane extremity.

2.1.4. Spread patterns measurements

Stationary spread patterns were measured with the rotating test bench (EN 13739–2, 2011) developed by Piron and Miclet (2005) and called CEMIB. This measurement device consisted of a rotating carrier and a motion less row of 80 collection trays. Each trays has a collection area of 0.5 × 0.5 m and is mounted on load cell. For the measurements, the revolution speed of the spreader carrier was 3°/s. During the rotation, the spread pattern passed over the row of trays, and the cumulated mass collected by each tray was recorded. The collected mass and the angular orientation of the carrier were simultaneously recorded with the acquisition frequency of 10 Hz. A specific algorithm had been developed to process the recorded data and to provide the 2-dimensional static spread pattern with a sampling interval of 0.25 × 0.25 m in Cartesian

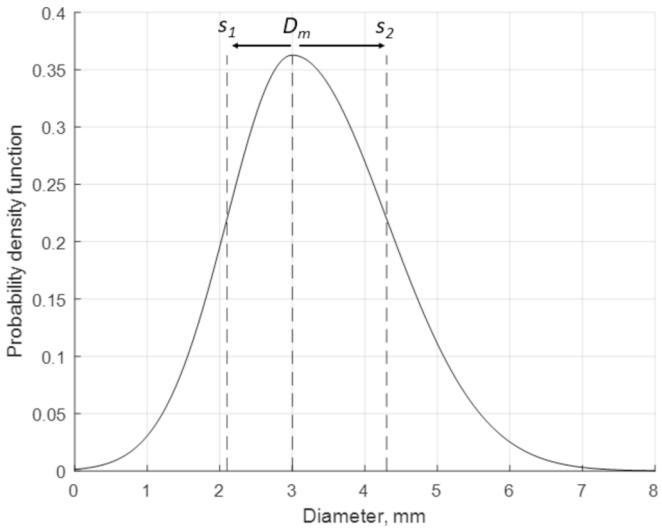

Fig. 4. Particle diameter distribution: example when $D_m = 3$, $s_1 = 0.9$ and $s_2 = 1.3$. From the right to the left, vertical dashed lines are placed at D_m-s_1, D_m and $D_m + s_2$ respectively.

coordinates with respect to the disk centre.

2.1.5. Particle size distribution measurement

Particle size distributions were measured using a videogranulometer. The device consisted of an inclined plate fed in its upper part by a flow of fertilizer particles. The plate was transparent and illuminated from the background. The feeding system provided a flow of separated particles crossing the plate and observed by a digital camera. The diameter of each particle was obtained using image processing so that the particle distribution of the fertilizer is deduced. Details concerning the measurement method are given in Le et al. (2018).

2.2. Actual and virtual fertilizers

2.2.1. Particle size distribution model

To describe particle size distributions, various models had been used in literature. Two-parameter distributions such as log-normal distribution (Gardner, 1956) or Rosin-Rammler distribution (Perfect et al., 1998) are widely used equations while more refined models had also been suggested, such as three- and four-parameter log-normal equations (Wagner and Ding, 1994) or five-parameter log-normal equation (Fredlund et al., 2000). In practice, the choice of the model is determined by striking a balance between the goodness of fit and the complexity of the model (*i.e.* number of parameters). Furthermore, the choice is determined by the possibility of easily interpreting the parameters in terms of distribution shape. Regarding this aspect, logarithmic models introduce dimensional and scaling changes, which complicate the parameter interpretation. Consequently, in this study, the probability density function $f(d)$ of particle diameters was modelled by a combination of two Gaussian membership functions as follows:

$$f(d) = \begin{cases} \dfrac{1}{(s_1 + s_2)}\sqrt{\dfrac{2}{\pi}}\exp\left(-\dfrac{1}{2}\left(\dfrac{d - D_m}{s_1}\right)^2\right) & \text{for } d \le D_m \\ \dfrac{1}{(s_1 + s_2)}\sqrt{\dfrac{2}{\pi}}\exp\left(-\dfrac{1}{2}\left(\dfrac{d - D_m}{s_2}\right)^2\right) & \text{for } d > D_m \end{cases} \quad (1)$$

where D_m is the modal value of the distribution (diameter value at which the probability density function attains its maximum value), s_1 and s_2 are the standard deviations of the right and left Gaussian membership functions respectively.

As illustrated in Fig. 4, the advantage of this model is to provide three meaningful parameters to describe independently the mode of the distribution, the dispersion of diameters smaller than the modal value and the dispersion of diameters higher than the modal value.

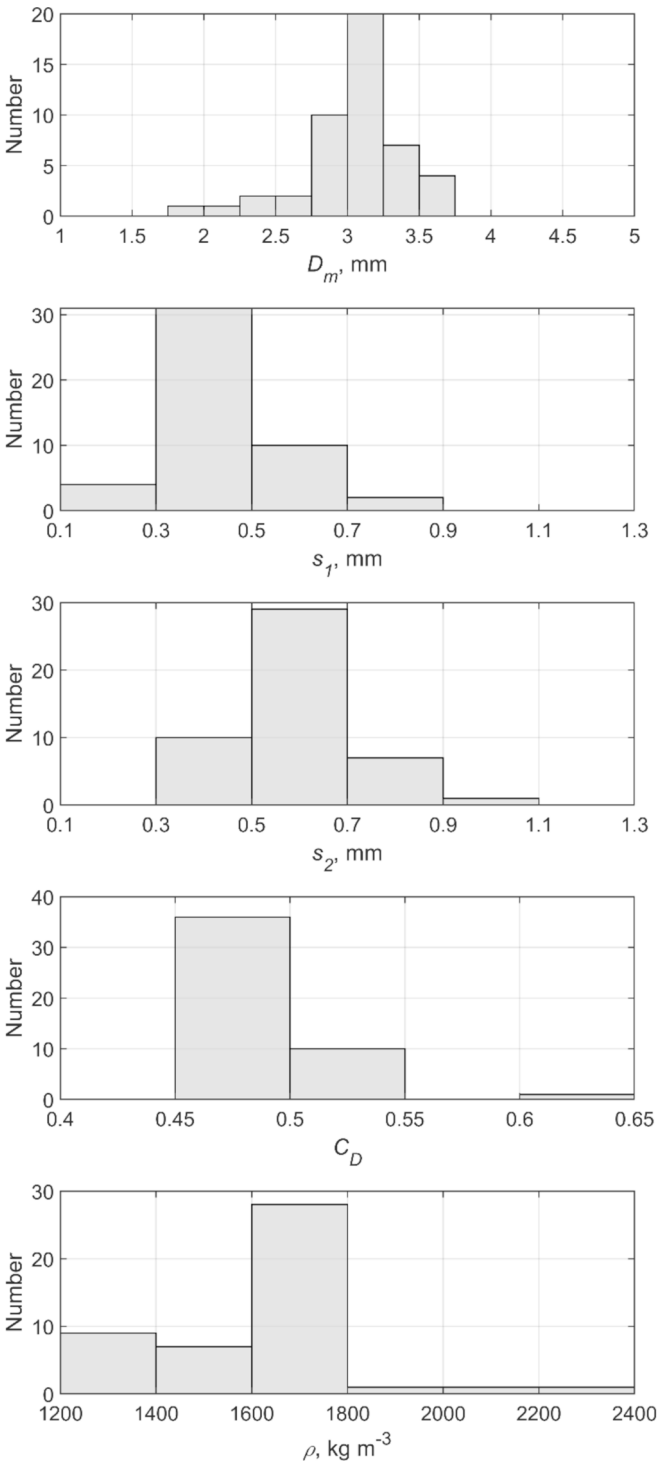

Fig. 5. Distribution histograms of the characteristic parameters measured for 47 commercially available fertilizers.

2.2.2. Actual fertilizers

Forty-seven commercially available fertilizers had been considered in this study. Their particle size distributions were analyzed using the videogranulometer presented in section 2.1.4. The measured values of D_m ranged from 1.9 to 3.7 mm, s_1 from 0.26 to 0.80 and s_2 from 0.39 to

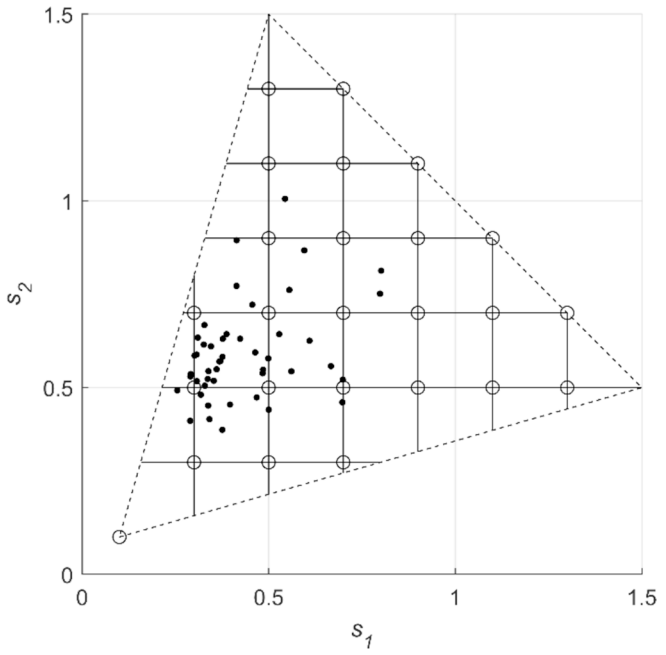

Fig. 6. Particle size distribution parameters (s_1 and s_2) measured for 47 commercially available fertilizers (·) and discretized pairs of values chosen to simulate virtual fertilizers (○).

1.01. The fertilizer specific density ρ was derived from weighing a fertilizer bulk volume and weighing the same bulk volume after completing with a liquid of known density, so that the particle mass and volume was deduced. The 47 measured values ranged from 1250 to 2320 kg m^{-3}.

The fertilizer drag coefficients C_D was deduced from spread patterns measured with the simplified disk SD (see section 2.1.1). For each fertilizer, the drag coefficient value was estimated by minimizing the difference between the measured spread pattern and computed spread patterns. This method had already been used by Villette et al. (2017) and Abbou-ou-cherif et al. (2017). The 47 measured values ranged from 0.45 to 0.62.

Fig. 5 presents the distribution histograms of the measured values for the five characteristic parameters and Fig. 6 presents the pairs of values (s_1, s_2) measured for each fertilizer.

2.2.3. Virtual fertilizers

In order to study the influence of fertilizer physical properties, a set of virtual fertilizers (combining different characteristics) was defined.

Concerning the particle size distribution, the investigated values for D_m were chosen from 1 to 5 in steps of 0.5 and the investigated values for s_1 and s_2 were chosen from 0.1 to 1.3 in steps of 0.2. To limit the number of virtual fertilizers, only certain paired values (s_1, s_2) were considered. These paired values (s_1, s_2) are in the triangle delimited by (0.1, 0.1), (0.5, 1.5) and (1.5, 0.5) as depicted in Fig. 6. Furthermore, to avoid unrealistic truncated distributions, the design of virtual fertilizers only considered pairs of values (s_1, s_2) for which $s_1 < D_m/3$. The combination of these discretized ranges of values and restrictions provided 152 triplets of values (D_m, s_1, s_2) describing 152 particle size distributions.

Accordingly to the distribution of the values obtained for actual fertilizers, the investigated range of values for C_D and ρ were chosen from 0.4 to 0.6 in steps of 0.05 and from 1200 to 2000 kg m^{-3} in steps of 200 kg m^{-3} respectively.

Combining 152 particle size distributions with 5 drag coefficient values and 5 density values, this provided 3800 virtual fertilizers with different physical characteristics, each defined by a 5-tuple of values (C_D, ρ, D_m, s_1, s_2).

Table 2
Values of parameters measured for urea and used to initiate ballistic flight simulations.

Parameters	Nomenclature	Long vane	Short vane
Horizontal outlet angle			
Mean value	$\mu\theta_{out}$	43.6°	
Standard deviation	$\sigma\theta_{out}$	1.1°	
Vertical outlet angle			
Mean value	$\mu\Omega_{out}$	7.8°	7.6°
Standard deviation	$\sigma\Omega_{out}$	1.0°	1.2°

2.3. Models and simulations

2.3.1. Virtual spreader

The study considered a virtual twin disk spreader composed of two disks with the right disk rotating counterclockwise and the left disk rotating clockwise. Both disks had the same revolution speed and were fed by the same fertilizer mass flow. In order to consider a realistic disk design, the characteristics of the virtual disk were taken from the S8 disk. Thus, the characteristics of the virtual disk were those of the S8 disk as specified in Table 1, including disk spacing set at 1.4 m.

2.3.2. Initial conditions of ballistic flight

In centrifugal spreading process, the initial conditions of the ballistic flight of the particles are defined by their locations when they leave the vane, their outlet velocities and directions.

In the Cartesian coordinate system (O, ***i***, ***j***, ***k***), the location of a particle (x_{out}, y_{out}, z_{out}) when it leaves the vane (Fig. 1) is as follows:

$$\begin{cases} x_{out} = r_i \times \cos\theta_{vane\ i} \\ y_{out} = r_i \times \sin\theta_{vane\ i} \\ z_{out} = h_i \end{cases} \quad (2)$$

where i is 1 for long vane and 2 for short vane, r_i is the radius of the vane, $\theta_{vane\ i}$ is the angular location of the vane, h_i is the height of the outer extremity of the vane.

According to Fig. 1, for a counterclockwise rotating disk, the horizontal angle of the particle trajectory is:

$$\theta_{traj} = \theta_{vane\ i} - \theta_{out} + \pi/2 \quad (3)$$

where θ_{out} is the horizontal outlet angle.

The components of the outlet velocity (vx_{out}, vy_{out}, vz_{out}) are as follows:

$$\begin{cases} vx_{out} = v_H \times \cos\theta_{traj} \\ vy_{out} = v_H \times \sin\theta_{traj} \\ vz_{out} = v_H \times \tan\Omega_{out} \end{cases} \quad (4)$$

where Ω_{out} are the vertical outlet angle and v_H is the horizontal component of the outlet velocity defined as follows:

$$v_H = \frac{r_i\omega}{\cos\theta_{out} + \sin\theta_{out}\tan\alpha_i} \quad (5)$$

where ω is the revolution speed of the disk and α_i is the pitch angle of the vane.

More details concerning the demonstrations of above equations can be found in Villette et al. (2008) and Villette et al. (2017).

To focus on the spreading ability of fertilizers, the study considered the same initial conditions of the ballistic flight for all fertilizers. This aligned with the assumption that spreader components can be designed and adjusted to achieve the desired ejection characteristics.

To ensure realistic conditions for simulations, the disk outlet characteristics were based on data measured with urea. Since the virtual disk was modeled from the S8 disk (section 2.1.1), outlet characteristics for the short and long vanes were required for spread pattern simulations. These data were deduced from measurements carried out with the S8S disk (equipped with short vanes) and the S8L disk (equipped with long

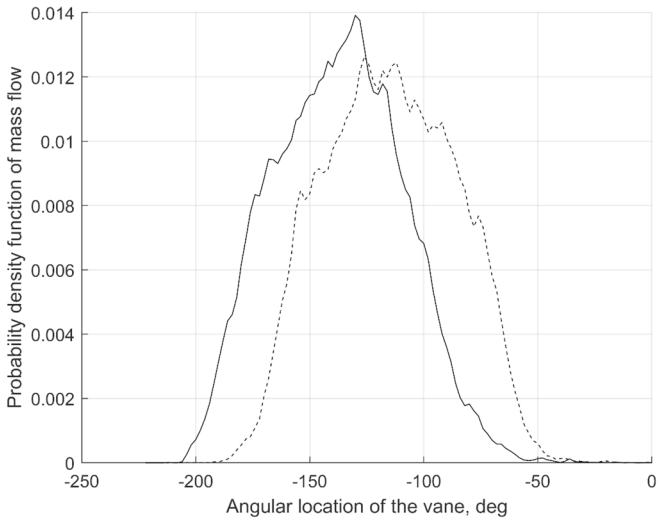

Fig. 7. Angular mass flow distribution measured with urea for the short vane (continuous line) and the long vane (dashed line). Mass flow distributions used to initiate ballistic flight simulations.

vanes) respectively. For all measurements, the spinning disks were mounted on the AXIS 50.1 spreader, the revolution speed was 900 rpm, the drop point index was 5 and the fertilizer mass flow was 1 kg/s.

The horizontal outlet angle was measured as described in section 2.1.2 for the disks S8S and S8L. As measured values were not significantly different, the same values were assumed for short and long vanes. This is in accordance with (Colin, 1997; Olieslagers, 1997; Villette et al., 2005). The mean value $\mu\theta_{out}$ and the standard deviation $\sigma\theta_{out}$ of the horizontal outlet angle are provided in Table 2.

The vertical distribution was measured as described in section 2.1.3 for the S8S and S8L disks. The mean values $\mu\Omega_{out}$ and the standard deviation $\sigma\Omega_{out}$ of the vertical outlet angle obtained for short (S8S) and long vanes (S8L) are provided in Table 2.

The angular distributions of the mass flow around the disks S8S and S8L were determined by analyzing stationary spread patterns measured for both disks as described in section 2.1.4. Fig. 7 presents the distributions obtained for short and long vanes. Details concerning the transformation of spread pattern into mass flow distribution can be found in Villette et al. (2017) and Abbou-ou-cherif et al. (2017).

2.3.3. *Ballistic flight model*

In this study, the ballistic flight model considers the gravity force and the drag force due to the motion of the particle through the air. This approach had been widely used by other researchers (Abbou-ou-cherif et al., 2017; Aphale et al., 2003; Griffis et al., 1983; Mennel and Reece, 1963; Olieslagers et al., 1996; Pitt et al., 1982; Villette et al., 2017), and described the motion of the particle by the following differential equations:

$$\begin{cases} \dfrac{d^2x}{dt^2} = -\dfrac{1}{2m} C_D A_p \rho_{air} vx \sqrt{vx^2 + vy^2 + vz^2} \\ \dfrac{d^2y}{dt^2} = -\dfrac{1}{2m} C_D A_p \rho_{air} vy \sqrt{vx^2 + vy^2 + vz^2} \\ \dfrac{d^2z}{dt^2} = -g - \dfrac{1}{2m} C_D A_p \rho_{air} vz \sqrt{vx^2 + vy^2 + vz^2} \end{cases} \quad (6)$$

where x ,y, z are the coordinates of the particle, m is the particle mass, C_D is the drag coefficient, A_p is the projected surface area of the particle, ρ_{air} is the air density (set at 1.21 kg m^{-3}), vx, vy, vz are the velocity components of the particle, g is the acceleration due to gravity.

In the model, the particle mass was related to the particle density ρ and diameter d as follows:

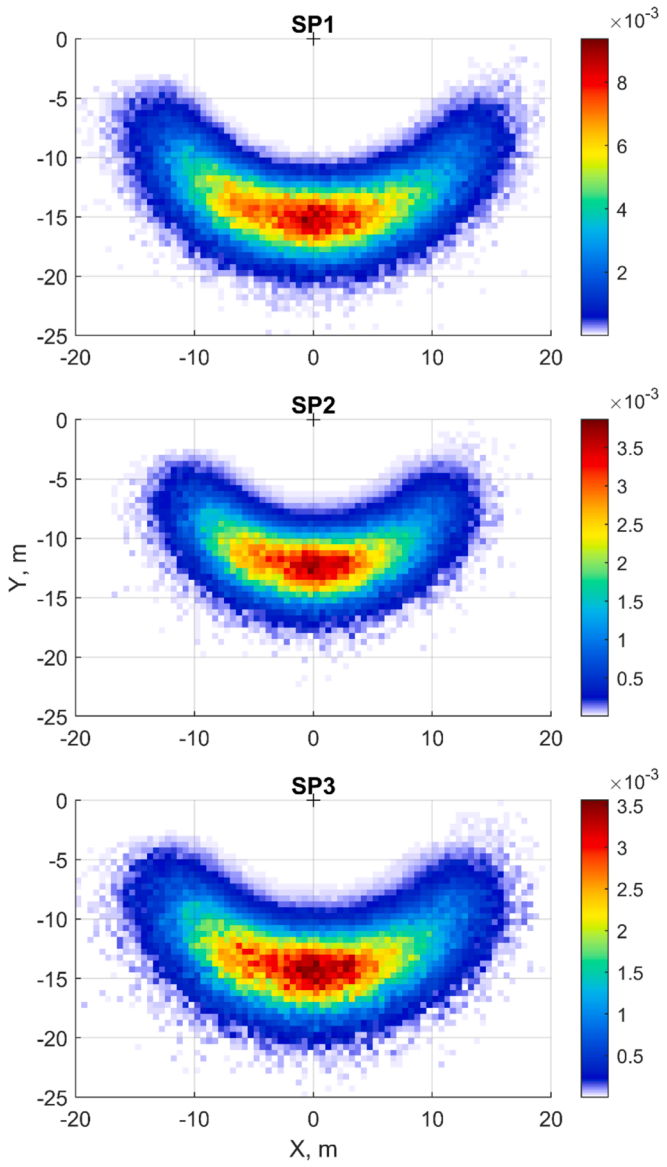

Fig. 8. Example of spread patterns simulated for the virtual right disk and three different virtual fertilizers. The spread pattern SP1 (top) was computed with C_D = 0.5, ρ=1400 kg m^{-3}, D_m = 3 mm, s_1 = 0.5 mm, s_2 = 0.5 mm; SP2 (middle) was computed with the same values except for D_m = 2 mm; SP3 (bottom) was computed with the same values except for D_m = 2 mm and ρ = 1800 kg m^{-3}. The cross (+) is the location of the disk center. The graduation of the color scale reflects the fertilizer mass (kg) lying on the sampling area (0.5 × 0.5 m). (For interpretation of the reference to color in this figure legend, the reader is referred to the web version of this article).

$$m = \rho \frac{4}{3} \pi \left(\frac{d}{2}\right)^2 \quad (7)$$

Thus, considering the same initial conditions for the ballistic flight, the fertilizer spread pattern depends on the aerodynamic drag coefficient C_D, the specific density ρ and the particle size distribution.

2.3.4. *Spread pattern simulations for one disk and R_m calculation*

The simulations used a Monte Carlo process to compute the motion of a large number of fertilizer particles. These particles were assigned several characteristics that were randomly drawn from pre-established statistical distributions. The algorithms were developed with Matlab (2015) software and utilized its built-in random number generator. For

variables following a normal distribution, the values were obtained using the *randn* function. In the case of other non-standard distributions, the selection of random values was performed in two steps. First, random numbers were generated with a uniform distribution using the *rand* function within the range of 0 to 1. Second, the final random values were deduced from these numbers by inversing the cumulative frequency function of the specified distribution.

For each virtual fertilizer defined by the 5-tuple (C_D, ρ, D_m, s_1, s_2), the corresponding stationary spread pattern was computed for the right disk of the virtual spreader. This was a counterclockwise disk modeled from the S8 disk as presented in Fig. 1 with parameters values as specified in Table 1. The landing locations of the particles were successively computed for each vane. Regarding the mass flow proportion p collected by each vane (Table 1), the number N of particles considered in the simulations was 100,000 particles ejected by the short vane and 75,439 by the long one. Therefore, for each vane, the simulations consisted of the following steps.

First, a collection of N virtual particles was generated by randomly selecting N values of diameter d from the size distribution defined by Eq. (1) and the assigned values of D_m, s_1 and s_2.

Second, the initial conditions for the ballistic flight were assigned to each particle, regardless of its diameter. For each particle, the values of the different variables were assigned as follows:

(1) The angular location of the vane θ_{vane} at the particle ejection time was randomly selected using the mass flow distribution (Fig. 7).
(2) The coordinates of the ejection point (x_{out}, y_{out}, z_{out}) were deduced from Eq. (2).
(3) The horizontal outlet angle θ_{out} was drawn from the normal distribution parametrized by $\mu\theta_{out}$ and $\sigma\theta_{out}$ (Table 2).
(4) The vertical outlet angle Ω_{out} was drawn from the normal distribution parametrized by $\mu\Omega_{out}$ and $\sigma\Omega_{out}$ (Table 2).
(5) The 3D-components of the outlet velocity (vx_{out}, vy_{out}, vz_{out}) were deduced from θ_{vane}, θ_{out} and Ω_{out} using Eqs. (3) to (5).

Third, the mass of each particle was computed (Eq. (7)) and the coordinates of the landing point of each particle were computed by solving Eq. (6) with the initial conditions of flight x_{out}, y_{out}, z_{out} and vx_{out}, vy_{out}, vz_{out}.

Cumulating all landing points for both vanes provided the simulated spread pattern for the right disk of the virtual spreader. Then, the mean radius R_m was calculated as the mean distance from the disk center to the landing points of all the particles ejected by the disk.

For example, Fig. 8 presents spread patterns computed for three different virtual fertilizers when the spreader travel direction is along the Y-axis. This illustrates how the spread pattern can be affected by the reduction of D_m (from SP1 to SP2) or the increase of ρ (from SP2 to SP3). This also illustrates how certain parameters (*e.g.* D_m and ρ) can compensate for each other to produce close spread patterns (comparing SP1 to SP3).

2.3.5. Twin disk spread pattern simulation and W_{WCV10} calculation

The spread pattern resulting from left disk was deduced from the right spread pattern by symmetry with respect to the spreader travel direction.

The setting of the virtual spreader consisted in rotating the right and left spread patterns around each disk from the same angle α_{set} counterclockwise for the right disk and clockwise for the left one. This simulated modifying the angular location of the feeding point on each disk. Finally, the twin disk spread pattern was deduced from associating the left and right spread patterns after translating the particle coordinates by half the disk spacing (1.4 m) in the left or right direction. The values of the setting angle ranged from 0° to 60° in steps of 1°.

For each spreader setting (*i.e.* each value of α_{set}), the transverse distribution is deduced from the twin disk spread pattern by considering a virtual row of collection trays aligned perpendicularly to the travel path of the virtual spreader. For a given working width W_W, several identical spread patterns were shifted right and left by multiples of W_W representing virtual adjacent passes and reproducing spread overlap. Depending on the transverse position of each particles of the spread patterns, the particles were affected to the corresponding virtual collection trays (0.5 × 0.5 m). Then, the transverse distribution of the fertilizer mass was determined by summing the mass collected by each tray, and the transverse coefficient of variation (CV) was calculated (EN 13739–2, 2011). For each virtual fertilizer, the setting map (Fig. 9) was finally created by storing the CV values in a matrix. In this matrix, rows represent different spreader settings α_{set}, and columns represent achievable working widths W_W. In order to assess the fertilizer ability to be spread on large width with a good uniformity, the indicator chosen to

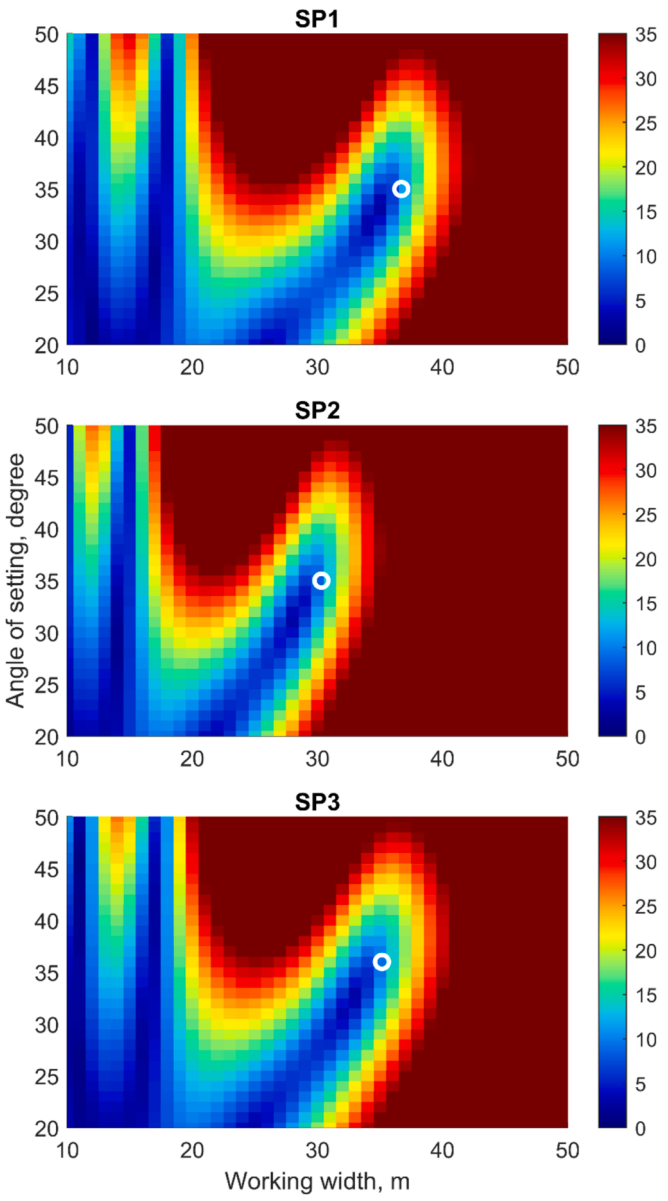

Fig. 9. Setting maps corresponding to the spread patterns SP1, SP2 and SP3 presented in Fig. 8 and obtained for three different virtual fertilizers. The spread pattern SP1 (top) was computed with $C_D = 0.5$, ρ=1400 kg m^{-3}, $D_m = 3$ mm, $s_1 = 0.5$ mm, $s_2 = 0.5$ mm; SP2 (middle) was computed with the same values except for $D_m = 2$ mm; SP3 (bottom) was computed with the same values except for $D_m = 2$ mm and $\rho = 1800$ kg m^{-3}. The color scale corresponds the value of the CV expressed in percentage. The largest working width respecting CV≤10 % is plotted (white circle). (For interpretation of the reference to color in this figure legend, the reader is referred to the web version of this article).

evaluate the performance was the maximum working width respecting CV≤10%, named W_{WCV10}. The choice of limiting the CV to 10 % to ensure good uniformity complies with standard EN 13739–1 (2011) which requires the CV does not exceed 15 %. The corresponding working width W_{WCV10}, was decuded from the setting map. First, the discretized value of the working width respecting the condition was deduced from the row value of the matrix and second, the refined value W_{WCV10} was estimated by linear interpolation between the two neighboring discrete values.

Fig. 9 illustrates the setting maps corresponding to the three virtual fertilizers for which single disk spread patterns were presented in Fig. 8. Fig. 9 shows that W_{WCV10} is 36.7 m when fertilizer properties are C_D = 0.5, ρ=1400 kg m^{-3}, D_m = 3 mm, s_1 = 0.5 mm and s_2 = 0.5 mm. W_{WCV10} decreases to 30.3 m when D_m is 2 mm. When D_m is maintained at 2 mm but ρ is increased to 1800 kg m^{-3}, W_{WCV10} increases anew to 35.2 m.

2.4. Regression model

The values of R_m and W_{WCV10} obtained from numerical simulations were utilized to create a model that directly relates these values to the physical characteristics of the particles: D_m, s_1, s_2, ρ, and C_D. The same model form was applied to both R_m and W_{WCV10}. First, a multivariate polynomial regression was performed for each of the 25 pairs of values (C_D, ρ) to determine the coefficients C_{Ri} and C_{Wi} (with i ranging from 1 to 7) for the models defined by Eqs. (8) and (9). As a result, 25 values were obtained for each of the seven C_{Ri} and C_{Wi} coefficients. Subsequently, each of these coefficients was modeled using multivariate linear regressions as described in Eqs. (10) and (11).

$$R_m = \begin{pmatrix} C_{R1}(\rho, C_D) \\ C_{R2}(\rho, C_D) \\ C_{R3}(\rho, C_D) \\ C_{R4}(\rho, C_D) \\ C_{R5}(\rho, C_D) \\ C_{R6}(\rho, C_D) \\ C_{R7}(\rho, C_D) \end{pmatrix}^T \times \begin{pmatrix} D_m^2 \\ D_m \\ D_m s_1 \\ D_m s_2 \\ s_1 \\ s_2 \\ 1 \end{pmatrix} \tag{8}$$

$$W_{WCV10} = \begin{pmatrix} C_{W1}(\rho, C_D) \\ C_{W2}(\rho, C_D) \\ C_{W3}(\rho, C_D) \\ C_{W4}(\rho, C_D) \\ C_{W5}(\rho, C_D) \\ C_{W6}(\rho, C_D) \\ C_{W7}(\rho, C_D) \end{pmatrix}^T \times \begin{pmatrix} D_m^2 \\ D_m \\ D_m s_1 \\ D_m s_2 \\ s_1 \\ s_2 \\ 1 \end{pmatrix} \tag{9}$$

$$C_{Ri}(\rho, C_D) = c_{Ri1}\rho + c_{Ri2}C_D + c_{Ri3} \tag{10}$$

$$C_{Wi}(\rho, C_D) = c_{Wi1}\rho + c_{Wi2}C_D + c_{Wi3} \tag{11}$$

Thanks to this model, the sensitivity analysis was performed by calculating the partial derivatives of R_m and W_{WCV10} with respect to the independent variables. The total derivative of R_m and W_{WCV10} are provided in Eqs. (12) and (13) respectively.

$$dR_m = \frac{\partial R_m}{\partial D_m}dD_m + \frac{\partial R_m}{\partial s_1}ds_1 + \frac{\partial R_m}{\partial s_2}ds_2 + \frac{\partial R_m}{\partial \rho}d\rho + \frac{\partial R_m}{\partial C_D}dC_D \tag{12}$$

$$dW_{WCV10} = \frac{\partial W_{WCV10}}{\partial D_m}dD_m + \frac{\partial W_{WCV10}}{\partial s_1}ds_1 + \frac{\partial W_{WCV10}}{\partial s_2}ds_2 + \frac{\partial W_{WCV10}}{\partial \rho}d\rho + \frac{\partial W_{WCV10}}{\partial C_D}dC_D \tag{13}$$

The analytical descriptions of the partial derivatives of R_m are provided in Eqs. (14) to (18), as follows:

$$\frac{\partial R_m}{\partial D_m} = 2C_{R1(\rho,C_D)}D_m + C_{R2(\rho,C_D)} + C_{R3(\rho,C_D)}s_1 + C_{R4(\rho,C_D)}s_2 \tag{14}$$

$$\frac{\partial R_m}{\partial s_1} = C_{R3(\rho,C_D)}D_m + C_{R5(\rho,C_D)} \tag{15}$$

$$\frac{\partial R_m}{\partial s_2} = C_{R4(\rho,C_D)}D_m + C_{R6(\rho,C_D)} \tag{16}$$

$$\frac{\partial R_m}{\partial \rho} = C_{R11}D_m^2 + C_{R21}D_m + C_{R31}D_m s_1 + C_{R41}D_m s_2 + C_{R51}s_1 + C_{R61}s_2 + C_{R71} \tag{17}$$

$$\frac{\partial R_m}{\partial C_D} = C_{R12}D_m^2 + C_{R22}D_m + C_{R32}D_m s_1 + C_{R42}D_m s_2 + C_{R52}s_1 + C_{R62}s_2 + C_{R72} \tag{18}$$

Similarly, partial derivatives of W_{WCV10} were obtained by substituting R_m with W_{WCV10} and C_{Ri} with C_{Wi} in Eqs. (14) to (18).

2.5. Experimental data for R_m and W_{WCV10}

Single disk spread patterns were measured for the 47 marketed fertilizers described in section 2.2.2. All spread patterns were measured with the rotating bench CEMIB as described in section 2.1.4 and with the counterclockwise S8 disk described in Table 1 and mounted on the AXIS 50.1 spreader. The revolution speed of the disk was 900 rpm. Theses 47 measured spread patterns were used to compute the experimental values of R_m *and* W_{WCV10} for the 47 fertilizers.

In order to simplify the use and processing of each spread pattern, it was considered as a 2-dimensional probability density function. Thus, the Cartesian coordinates of a set of 300,000 identical particles was randomly drawn from this 2D probability density function to model the fertilizer mass distribution on the ground. The major advantage of this method is to avoid complex interpolation and resampling on square grids when rotation or translation of spread patterns is required (to reproduce working width setting, overlapping adjacent passes or transverse distributions).

Using this approach, the mean radius R_m of the single disk spread pattern was simply computed as the mean distance between the disk centre and the coordinates of all the particles representing the spred pattern.

Table 3
Numerical values of the model coefficients for R_m.

i	C_{Ri1}	C_{Ri2}	C_{Ri3}	R^2
1	−1,0153E-04	3,2029E-01	−1,8406E-01	0,991
2	1,4628E-03	−4,4746E + 00	4,3079E + 00	0,995
3	3,1722E-05	−1,2102E-01	5,7649E-03	0,898
4	−2,9331E-04	8,6892E-01	−8,3262E-01	0,994
5	−4,2673E-04	1,3983E + 00	−9,8010E-01	0,988
6	1,6275E-03	−4,9057E + 00	5,9312E + 00	0,992
7	2,2784E-03	−7,1467E + 00	4,1132E + 00	0,988

Table 4
Numerical values of the model coefficients for W_{WCV10}.

i	C_{Wi1}	C_{Wi2}	C_{Wi3}	R^2
1	−1,7777E-04	5,7200E-01	−3,3673E-01	0,985
2	3,1687E-03	−9,9546E + 00	9,5001E + 00	0,995
3	−1,4341E-04	4,7779E-01	−4,6515E-01	0,984
4	−6,6163E-04	2,0399E + 00	−1,9029E + 00	0,989
5	0	0	0	
6	3,9057E-03	−1,1921E + 01	1,4189E + 01	0,992
7	5,2146E-03	−1,5929E + 01	9,9869E + 00	0,988

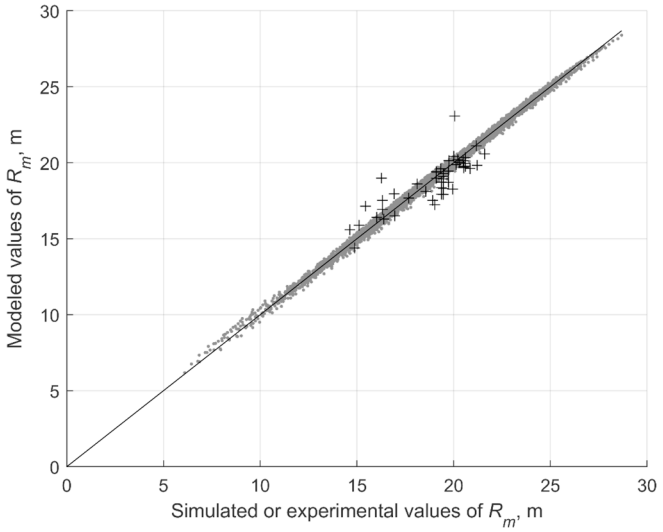

Fig. 10. Modeled values of R_m with respect to values computed through numerical simulations (·) or experimental values (+). The continuous line is the identity line.

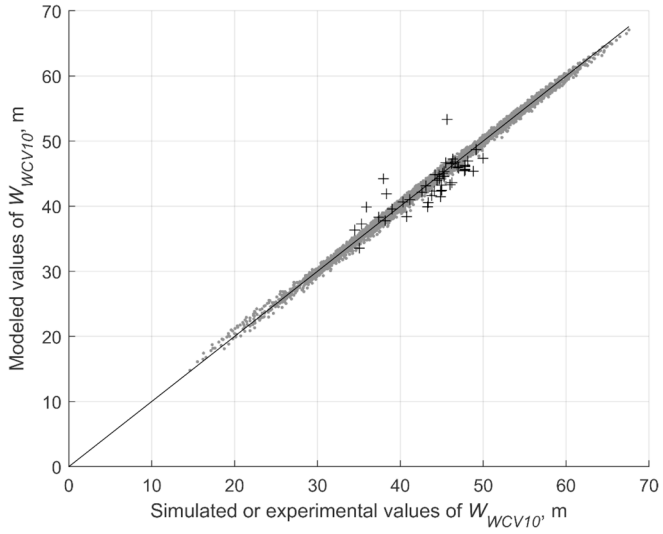

Fig. 11. Modeled values of W_W with respect to values computed through numerical simulations (·) or experimental values (+). The continuous line is the identity line.

The maximum working width W_{WCV10} was computed from the measured single spread pattern by reproducing the setting of the AXIS 50.1 spreader. For this spreader, the setting of the working width is obtained by adjusting the angular location of the drop point onto the disk. As rotating the drop point rotates the spread pattern around the disk, the setting principle is exactly the same that the setting of the virtual spreader used in this study. Using the description of the spread pattern as a set of identical particles, the maximum working width W_{WCV10} was computed from the measured spread pattern following the method described in section 2.3.5.

3. Results and discussion

The mean radius R_m of spread patterns and the maximum working widths W_{WCV10} respecting CV≤10%, have been computed for 3800 virtual fertilizers combining 152 particle size distributions (defined by D_m, s_1, s_2), 5 drag coefficient values (C_D) and 5 density values (ρ). Models for R_m and W_{WCV10} have been fitted to simulated data (section 3.1), compared to experimental data (section 3.2) and used to assess how the physical properties of particles influence the spreading performances of fertilizers (section 3.3).

3.1. Data fitting and model coefficients

3.1.1. Model coefficients for R_m

According to Eq. (8), the coefficients C_{Ri} (with i ranging from 1 to 7) were calculated using the least squares method and fitting R_m to the values obtained from numerical simulations. These coefficients were calculated for each pair of values (C_D, ρ). In all 25 regressions, the coefficients of determination (R^2) were found greater than 0.997.

Each of the 7 coefficients C_{Ri} was subsequently fitted as a function of ρ and C_D according to Eq. (10). The values for coefficients C_{Ri1}, C_{Ri2}, C_{Ri3} (with i ranging from 1 to 7) and the corresponding determination coefficients are provided in Table 3. The coefficients of determination are all greater than 0.98, except for the fitting of C_{R3}. To improve the modeling of C_{R3}, the inclusion of the quadratic terms ρ^2, C_D^2, and the interaction term $\rho\ C_D$, could be considered. With these three additional terms, the determination coefficient would exceed 0.98. However, due to the satisfactory predictive quality (Fig. 10) of R_m obtained from Eqs. (8) and (10), this improvement was deemed unnecessary and is not accounted for in this analysis. In Fig. 10, the modeled values of R_m are presented with respect to the values obtained from the numerical simulations with the 3800 virtual fertilizers. The coefficient of determination is then 0.997. The mean of the relative differences between modeled and simulated values is 0.95 % and 90 % of the differences are lower than 2.0 %.

3.1.2. Model coefficients for W_{WCV10}

The modeling of W_{WCV10} was conducted in a similar manner as explained earlier for R_m. However, due to a low coefficient of determination obtained for the expression of C_{W5}, the variable s_1 was not considered in the modeling of W_{WCV10}. To maintain a consistent and general form shared by the modeling of both R_m (Eq. (8)) and W_{WCV10} (Eq. (9)), the coefficient C_{W5} was therefore set to 0. Under these conditions, the coefficients of determination obtained for modeling W_{WCV10} with each of the 25 pairs of values (C_D, ρ) are all greater than 0.997. The coefficients C_{Wi1}, C_{Wi2}, C_{Wi3} (with i ranging from 1 to 7) and the corresponding determination coefficients are provided in Table 4. The values of C_{W51}, C_{W52} et C_{W53} were also set to zero, consistent with the imposed zero value for C_{W5}. Fig. 11 presents the values of W_{WCV10} derived from

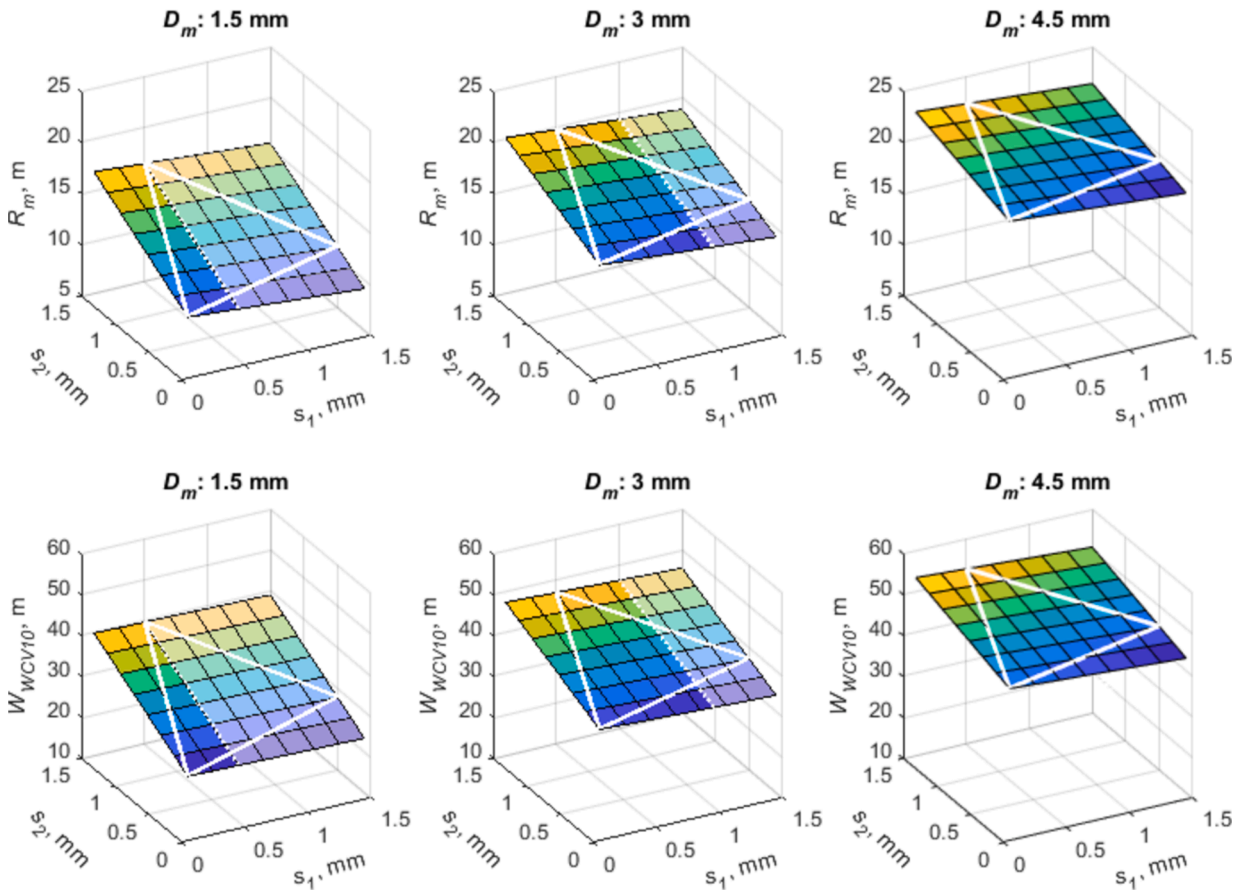

Fig. 12. R_m (top row) and W_{WCV10} (bottom row) as functions of s_1 and s_2, from three values of D_m (from left to right). The white triangle delimits the area of parameter values covered by simulations. The white dotted line delimits the area where $s_1 < D_m/3$.

the model (Eqs. (9) & (11)) with respect to the values computed by numerical simulations, with a coefficient of determination of 0.997. The mean of the relative differences between modeled and simulated values is 0.96 % and 90 % of the differences are lower than 2.0 %.

3.1.3. Limit of use of the coefficients

The coefficients provided in Tables 3 & 4 were derived from simulations performed with fixed disk characteristics. These voluntary fixed spreader parameters were chosen to isolate the effect of fertilizer properties during the spreading process independently from initial ballistic flight conditions that can be adapted by modifying disk design. This ensure unbiased comparisons of fertilizer abilities. Thus, the predicted values calculated with the coefficient matrices given in Tables 3 & 4 suite for comparing fertilizer spreading ability and evaluating the respective contribution of the different physical properties. They are not intended to predict the absolute working width achievable with different spreaders.

3.2. Comparison to experimental data

Spreading performances (R_m and W_{WCV10}) were also calculated using the models (Eqs. (8) and (9)) with the coefficients determined in Tables 3 and 4, and the physical characteristics measured for the 47 actual fertilizers described in section 2.2.2. The calculated values have been represented in Figs. 10 and 11 according to the experimental values obtained for R_m and W_{WCV10} (section 2.5).

The figures show greater disparities between modeled and experimental values for actual fertilizers compared to the disparities observed between modeled and simulated values. For R_m, the mean of the relative differences between modeled and simulated values is 4.3 % and 90 % of the differences are lower than 8.0 %. For W_{WCV10}, the mean is 4.1 % and 90 % of the differences are lower than 7.6 %.

These greater differences highlight that the model aims to evaluate the ballistic abilities of the product and not to model its behavior over the entire centrifugal spreading process (on– and off-the-disk). Thus, the simulations were deliberately performed by considering identical initial ballistic flight conditions for all fertilizer particle size distributions. This ensures the assessment of fertilizer spreading performances regardless of spreader characteristics. On the opposite, when experimental spread patterns are used, the values deduced for R_m and W_{WCV10} are not only affected by the behavior of the fertilizer particles during ballistic flight but also by their interaction with the spinning disk. Thus, the dispersion obtained from data derived from actual measurements is not surprising taking into account differences in outlet disk conditions (*i.e.* outlet angles and mass flow distribution) for actual tests. This also illustrates the interest of numerical simulations to study the ability of fertilizer to be spread without bias induced by machine parameters.

Additionally, although the model does not take into account the specific disk outlet conditions of each actual fertilizer, it is worth noting that the values of R_m and W_{WCV10} deduced from the experimental data remain consistent with the model.

3.3. Fertilizer spreading performance analysis

3.3.1. Influence of particle size distribution

Considering a density ρ of 1500 kg/m3 and a drag coefficient C_D of 0.5, Fig. 12 illustrates the influence of particle size distributions on R_m and W_{WCV10}. In order to improve the visibility of trends according to s_1 and s_2, the values were represented over the entire range of values going from 0 to 1.5 mm. The area covered by the pairs of values (s_1, s_2) used in

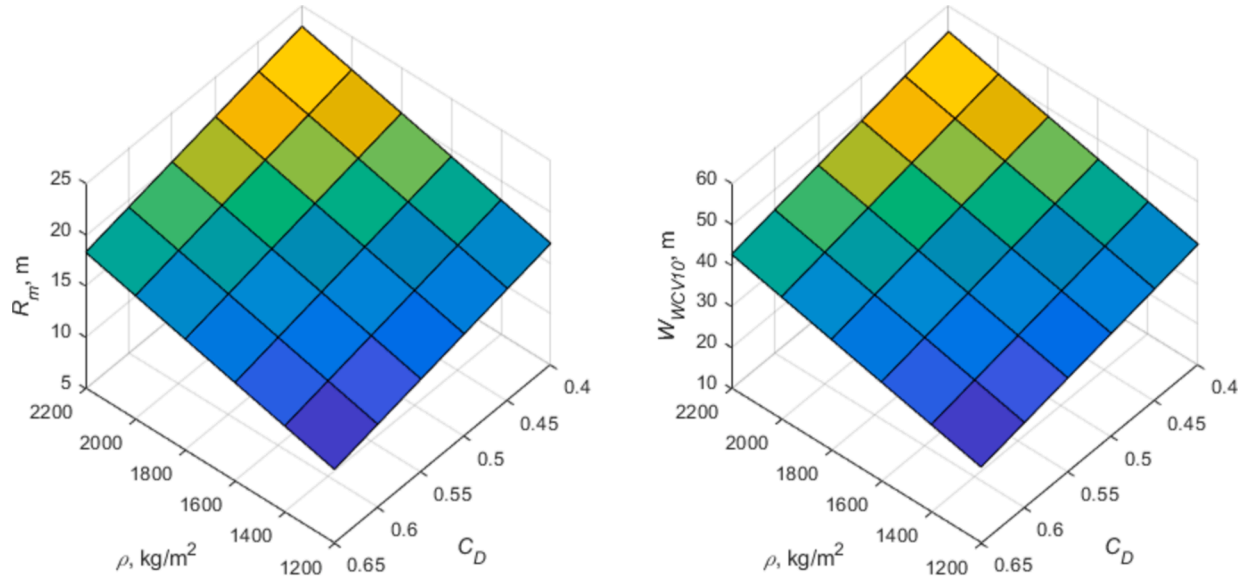

Fig. 13. R_m (left) and W_{WCV10} (right) as functions of ρ and C_D, for a particle size distribution defined by $D_m = 3$, $s_1 = 0.4$ and $s_2 = 0.6$.

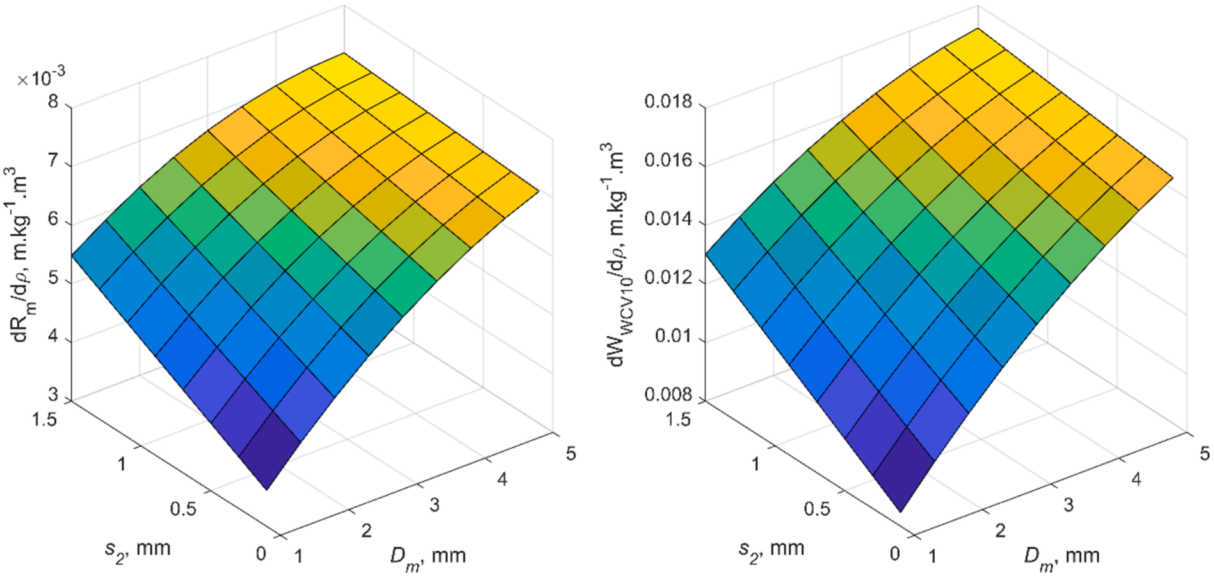

Fig. 14. Sensitivity to the density ρ of R_m (left) and W_{WCV10} (right) as a functions of D_m and s_2 for a value of s_1 set at 0.4 mm.

simulations is delimited by a triangle. This triangle corresponds to the choice of the study area in accordance with usual particle size distributions (Fig. 6). Fig. 12 shows that the trends observed for R_m and W_{WCV10} are similar. First, R_m and W_{WCV10} increase with the D_m. This trend is consistent since larger particle diameters result in greater mass, higher energy acquired during ejection, and longer ballistic flight length (assuming other parameters remain constant). Second, it shows that an increase in s_2 leads to an increase in R_m and W_{WCV10}, while an increase in s_1 results in a decrease in R_m and W_{WCV10}. This trend is linked to the increase in the number of large particles ($d > D_m$) projected far from the disk when s_2 increases, and the increase in the number of small particles ($d < D_m$) projected closer to the disk when s_1 increases. Third, the figure demonstrates that the influence of s_2 is much more significant than that of s_1. This is explained by the asymmetric effect of s_1 and s_2 in terms of mass of particles projected closer or farther from the disk. Thus, the same increase in particle count produces a greater mass if it concerns larger diameters than smaller diameters. Fourth, the higher the initial values of R_m and W_{WCV10}, the less impact the same absolute variations of s_1 and s_2 have on R_m and W_{WCV10}. Since the elevated values of R_m and W_{WCV10} result from higher values of D_m, the relative impacts of s_1 and s_2 in relation to D_m are consequently diminished.

3.3.2. *Influence of density and drag coefficient*

Fig. 13 presents the evolution of R_m and W_{WCV10} as a function of the density and the drag coefficient for an example of particle size distribution defined by: $D_m = 3$, $s_1 = 0.4$ and $s_2 = 0.6$. The variations of R_m and W_{WCV10} should be compared to those presented in Fig. 12 concerning the impact of particle size distribution. The variations of R_m and W_{WCV10} as functions of ρ and C_D demonstrate the strong influence of these two parameters on spreading performances.

Fig. 14 presents the sensitivity of R_m and W_{WCV10} to density (Eq. (17)) as a function of predominant particle size parameters affecting spreading performance, namely D_m and s_2. Similarly, Fig. 15 demonstrates the sensitivity of R_m and W_{WCV10} to the drag coefficient C_D (Eq. (18)). The observed trends for R_m and W_{WCV10} are similar. Bulk density has a positive effect on R_m and W_{WCV10} ($dR_m/d\rho > 0$ and $dW_{WCV10}/d\rho >$

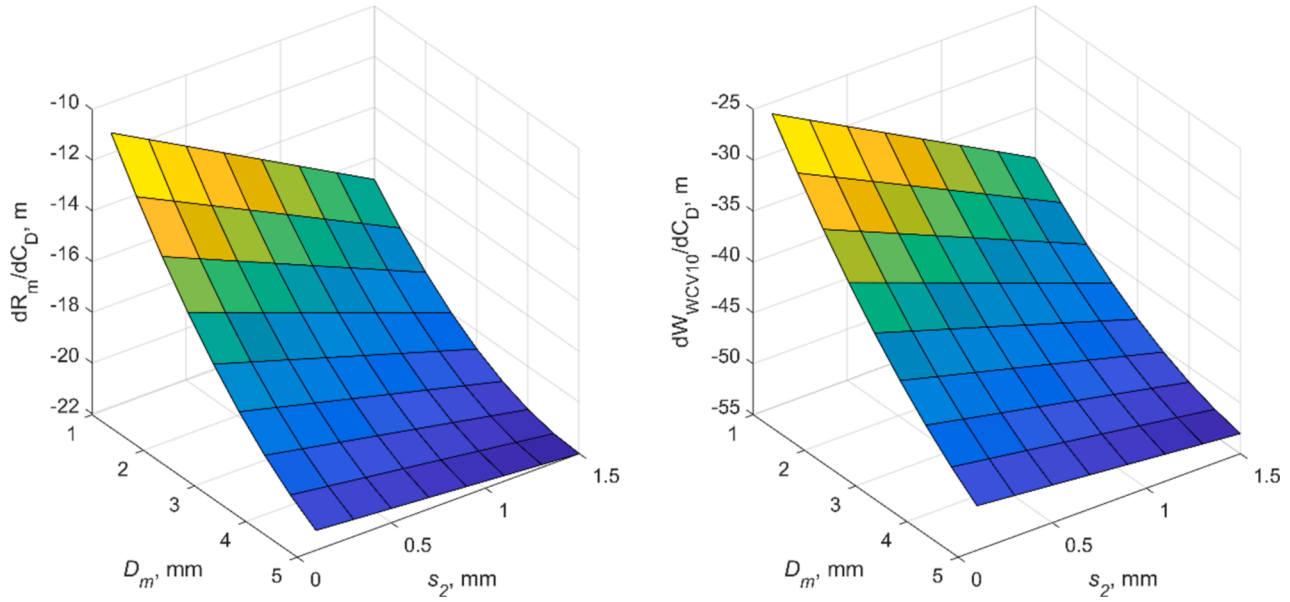

Fig. 15. Sensitivity to the drag coefficient C_D of R_m (left) and W_{WCV10} (right) as a function of D_m and s_2 for a value of s_1 set at 0.4 mm.

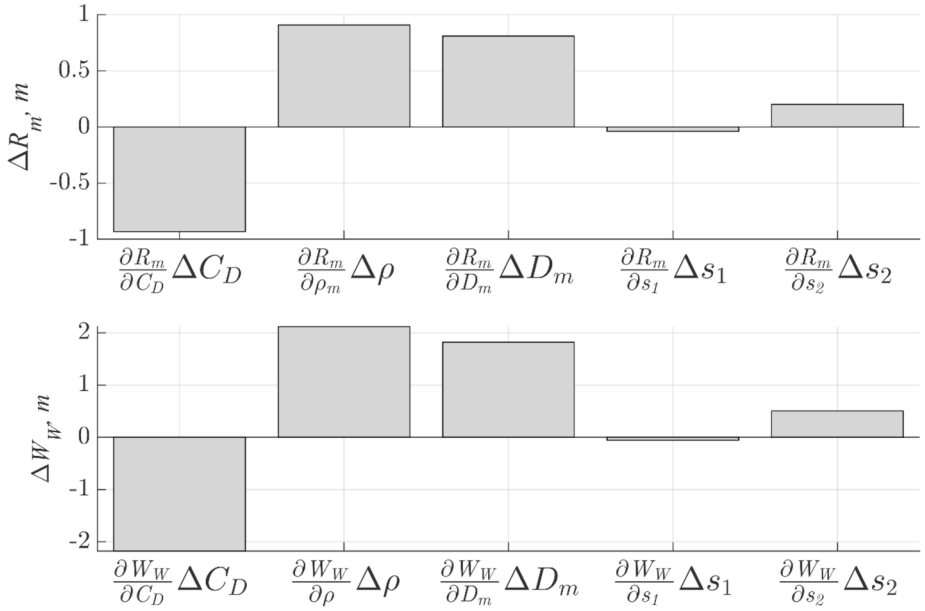

Fig. 16. Variations of R_m (top) and W_{WCCV10} (bottom) related to 10 % of variation for each parameter when the initial values are $D_m = 3$ mm, $s_1 = 0.4$ mm, $s_2 = 0.6$ mm, $\rho = 1500$ kg/m3, and $C_D = 0.5$.

0), and the increase in R_m and W_{WCV10} resulting from an increase in ρ is more significant when D_m and s_2 are larger. On the other hand, the drag coefficient has a negative effect on R_m and W_{WCV10} ($dR_m/d\rho < 0$ and $dW_{WCV10}/d\rho < 0$). The impact of the drag coefficient in terms of reduction on R_m and W_{WCV10} is more significant as D_m increases. The impact also increases with s_2. The influence of s_2 on the sensitivity of R_m and W_{WCV10} to C_D is attenuated when s_2 decreases in proportion to D_m.

This also illustrates how the sensitivity of the maximum working width to fertilizer properties can be easily visualized thanks to the models derived from simulated data.

3.3.3. Analysis and visualization of each parameter contribution

As illustrated above, Eqs. (14) to (18) or equivalent forms for W_{WCV10}, provide the sensitivity of R_m and W_{WCV10} to each parameter. In addition, Eqs. (12) and (13) decompose the overall variation of R_m or W_{WCV10} based on the variation of each model parameter. For instance, let's consider a 10 % increase in the value of each of these parameters compared to an initial situation defined by $D_m = 3$ mm, $s_1 = 0.4$ mm, $s_2 = 0.6$ mm, $\rho = 1500$ kg/m3, and $C_D = 0.5$. Fig. 16 presents the consequences of this increase on R_m and W_{WCV10} by analyzing the contribution of each parameter. A 10 % increase in the drag coefficient results in a reduction of approximately 2 m in the working width W_{WCV10} that can be counterbalanced by a 10 % increase in the density, which also results in an increase of approximately 2 m in W_{WCV10}. Regarding the particle size distribution parameters, the figure once again demonstrates that D_m is the most significant parameter. The impact of s_2 is less pronounced, while the impact of s_1 is negligible. The 10 % variation, applied to the input variables in this example, is used for illustrative purposes independently of the maximum amplitude of variation possible for each parameter and the practical difficulties of modifying the values of these

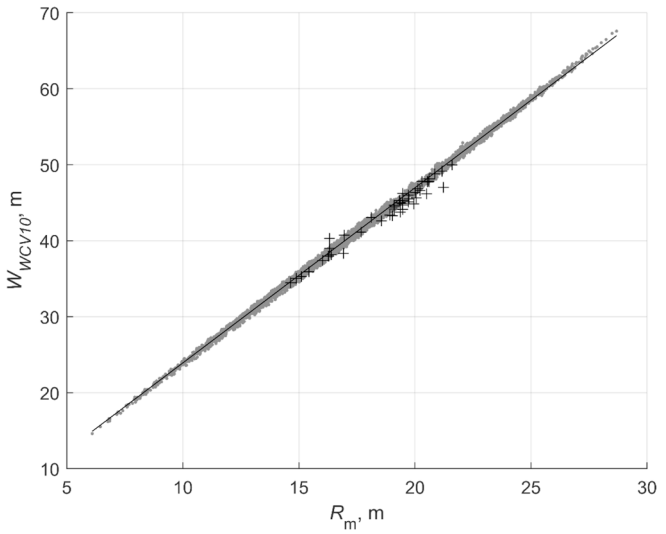

Fig. 17. Simulated values (·) and experimental values (+) of W_{WCV10} with respect to R_m.

parameters. Nevertheless, this example highlights the value of the model in assisting fertilizer producers in making the choice of product physical characteristics to compare or improve fertilizer spreading ability. For instance, this finding demonstrates that screening fertilizers to reduce the particle size dispersion has no benefit in improving fertilizer spreading ability, since s_1 has negligible effect and s_2 has a beneficial effect.

Since the numerical simulations have been carried out beforehand, the use of the established model does not require computing power and can be easily integrated into any type of software, such as spreadsheet. Moreover, the use of such an application is not limited to fertilizers but concerns all granular products spread using centrifugal process.

3.3.4. *Relationship between R_m and W_{WCV10}*

Using numerical simulation results, Fig. 17 demonstrates W_{WCCV10} is directly correlated to R_m. The linear regression (with $R^2 > 0.998$) is as follows:

$$W_{WCV10} = 2.305R_m + 0.87 \tag{19}$$

Actual values obtained for 47 commercially available fertilizers have also been plotted. Despite a more limited range of explored values and scatted results, the experimental values align with the simulated results and also support that W_{WCCV10} is correlated to R_m (with $R^2 > 0.968$). These findings demonstrate the necessity of a large mean radius of the spread pattern to achieve a wide working width while maintaining uniform spreading (CV≤10%).

4. Conclusions

The study demonstrates that the use of computer simulations is a relevant way to assess the ability of fertilizer to be spread on large working width. Considering 3800 virtual fertilizers, the advantage of the approach is to provide large amount of data, from which models can be derived. Another advantage is to isolate the influence of fertilizer properties from the effects of fertilizer-spreader interactions and spreader performance. Thanks to the large amount of simulated data, models are developed for the first time to relate the maximum working width and the mean radius of the spread pattern to 5 fertilizer physical properties: drag coefficient, specific density and three parameters describing the diameter distribution. Thereby, the study provides an analytical model to quantify the contribution of each of these five variables using partial derivatives. The drag coefficient, the specific density and the modal diameter of particle size distribution appear as key parameters.

The correlation between the maximum working width and the mean radius of the spread pattern is also demonstrated.

The model derived from numerical simulations provides fertilizer producers with an efficient tool. This tool enables them to make informed decisions about the particle physical properties required to achieve a specific level of fertilizer spreading performance. This is of practical use to guide the physical property design of new fertilizers, which are constantly being developed to reach more efficiency and reduce impacts on the environment, such as the development of granular organic fertilizer. In addition, the findings are not limited to fertilizers but concern all granular materials spread using centrifugal processes such as seeds for broadcast sowing.

Further researches will include the study of how fertilizer properties influence the robustness of the spread pattern, this means how fertilizer properties affect the spread pattern's ability to maintain acceptable uniformity as the working width deviates from its optimal value.

CRediT authorship contribution statement

Tien-Thinh Le: Validation, Software, Methodology, Investigation. **Emmanuel Piron:** Writing – review & editing, Validation, Methodology, Funding acquisition, Conceptualization. **Denis Miclet:** Methodology, Investigation. **Sylvain Villette:** Writing – original draft, Visualization, Formal analysis.

Declaration of competing interest

The authors declare that they have no known competing financial interests or personal relationships that could have appeared to influence the work reported in this paper.

Acknowledgements

The work was supported by YARA Company (Norway) and the French Research National Institute for Agriculture, Food and Environment (INRAE). The authors acknowledges the support received from the Agence Nationale de la Recherche of the French government through the program "Investissements d'Avenir'' (16-IDEX-0001 CAP 20-25). The authors gratefully acknowledge RAUCH Company (Germany) for providing the spreader and the spinner disks.

Data availability

The authors do not have permission to share data.

References

Abbou-ou-cherif, E.M., Piron, E., Chateauneuf, A., Miclet, D., Lenain, R., Koko, J., 2017. On-the-field simulation of fertilizer spreading: Part 1 – modeling. Comput. Electron. Agric. 142 (Part A), 235–247.

Antille, D.L., Gallar-Redondo, L., Godwin, R.J., 2013. Determining the particle size range of organomineral fertilisers based on the spreading characteristics of the material, ASABE Annual International Meeting. American Society of Agricultural and Biological Engineers, Kansas City, Missouri, p. 18.

Aphale, A., Bolander, N., Park, J., Shaw, L., Svec, J., Wassgren, C., 2003. Granular fertiliser particle dynamics on and off a spinner spreader. Biosyst. Eng. 85, 319–329.

Colin, A., 1997. Etude du procédé d'épandage centrifuge d'engrais minéraux [Study of the centrifugal spreading process of fertilizer]. Université de Technologie de Compiègne, France.

EN 13739-1, 2011. Agricultural machinery - Solid fertilizer broadcasters and full width distributors - Environmental protection - Part 1: Requirements, European Committee for Standardization, Bruxelles.

EN 13739-2, 2011. Agricultural machinery - Solid fertilizer broadcasters and full width distributors - Environmental protection - Part 2: Test methods, European Committee for Standardization, Bruxelles.

Fredlund, M.D., Fredlund, D.G., Wilson, G., 2000. An equation to represent grain-size distribution. Canad. Geotech. J. 37, 817–827.

Fulton, J.P., Thaper, R.K., Virk, S.S., McDonald, T., Fasina, O., 2020. Effect of vane shape on fertilizer distribution for a dual-disc spinner spreader. Appl. Eng. Agric. 36, 743–751.

Gardner, W.R., 1956. Representation of soil aggregate-size distribution by a logarithmic-normal distribution. Soil Sci. Soc. Am. J. 20, 151–153.
Grafton, M., Yule, I., Robertson, B., Chok, S., Manning, M., 2015. Ballistic modeling and pattern testing to prevent separation of new zealand fertilizer products. Appl. Eng. Agric. 31.
Griffis, C., Ritter, D., Matthews, E., 1983. Simulation of rotary spreader distribution patterns. Trans. ASAE 26, 33–37.
Gyldengren, J., Greve, M.B., Skou-Nielsen, N., Olesen, J.E., Gislum, R., 2020. Field scale agronomic and environmental consequences of overlapping N fertilizer application by disc spreaders. Field Crops Res. 255, 107901.
Heppler, K., 1993. Parameterstudien zur Granulatausbringung mit Schleuderscheiben.[A parameter study on granular fertiliser distribution by centrifugal spreaders.]. Facultät für Maschinenbau der Universität Karlsruhe (TH), Germany, p. 200. PhD Thesis.
Hoffmeister, G., Watkins, S., Silverberg, J., 1964. Fertilizer consistency, bulk blending of fertilizer material: effect of size, shape, and density on segregation. J. Agric. Food Chem. 12, 64–69.
Hofstee, J.W., 1995. Handling and spreading of fertilizers: part 5, the spinning disc type fertilizer spreader. J. Agric. Eng. Res. 62, 143–162.
Hofstee, J.W., Huisman, W., 1990. Handling and spreading of fertilizers part 1: physical properties of fertilizer in relation to particle motion. J. Agric. Eng. Res. 47, 213–234.
Le, T.-T., Miclet, D., Heritier, P., Piron, E., Chateauneuf, A., Berducat, M., 2018. Morphology characterization of irregular particles using image analysis. application to solid inorganic fertilizers. Comput. Electron. Agric. 147, 146–157.
Matlab, 2015. Version 8.5. The MathWorks, Inc., Natick, Massachusetts, United States., The MathWorks, Inc., Natick, Massachusetts, United States.
Mennel, R., Reece, A., 1963. The theory of the centrifugal distributor III: particle trajectories. J. Agric. Eng. Res. 7, 78–84.
Miller, P.C., Audsley, E., Richards, I.R., 2009. Costs and effects of uneven spreading of nitrogen fertilisers, Conference of the International Fertiliser Society, Cambridge, UK, 10th December 2009. International Fertiliser Society, pp. 1-24.
Miserque, O., Pirard, E., Schenkel, Y., Mostade, O., Huyghebaert, B., 2008. Spreading segregation of blended fertilizers: influence of the particles properties. Appl. Eng. Agric.
Olieslagers, R., Ramon, H., De Baerdemaeker, J., 1996. Calculation of fertilizer distribution patterns from a spinning disc spreader by means of a simulation model. J. Agric. Eng. Res. 63, 137–152.
Olieslagers, R., 1997. Fertilizer distribution modelling for centrifugal speader design. PhD Thesis, nr. 341. aan de faculteit der landboowwetenschappen, K. U. Leuven, Belgium.
Parkin, C., Basford, B., Miller, P., 2005. Spreading accuracy of solid urea fertilisers. DEFRA report NT2610. Dept. Environment, Food, Rural Affairs., London, UK.
Perfect, E., Xu, Q., Terry, D.L., 1998. Improved parameterization of fertilizer particle size distribution. J. AOAC Int. 81, 935–942.
Persson, K., 1996. Interactions between fertilisers and spreaders, Conference of the Fertiliser Society. The Fertiliser Society, Cambridge, UK, p. 28.
Piron, E., Miclet, D., 2005. Centrifugal fertiliser spreaders: a new method for their evaluation and testing, Conference of the International Fertiliser Society, York, United Kingdom. The International Fertiliser Society, p. 22p.
Pitt, R., Farmer, G., Walker, L., 1982. Approximating equations for rotary distributor spread patterns. Trans. ASAE 25, 1544–1552.
Richards, I.R., Hobson, R.D., 2013. Method of calculating effects of uneven spreading of fertiliser nitrogen. International Fertiliser Society Proc. No. 734.
Thaper, R.K., Fulton, J.P., McDonald, T.P., Fasina, O.O., 2021. Potential of fertilizer segregation during application using spinner disc spreader. Precis. Agric.
Tissot, S., Miserque, O., Mostade, O., Huyghebaert, B., Destain, J., 2002. Uniformity of N-fertiliser spreading and risk of ground water contamination. Irrigat. Drain. 51, 17–24.
Villette, S., Piron, E., Cointault, F., Chopinet, B., 2005. Centrifugal spreading: an analytical model for the motion of fertiliser particles on a spinning disc. Biosyst. Eng. 92, 157–164.
Villette, S., Piron, E., Cointault, F., Chopinet, B., 2008. Centrifugal spreading of fertiliser: Deducing three-dimensional velocities from horizontal outlet angles using computer vision. Biosyst. Eng. 99, 496–507.
Villette, S., Piron, E., Miclet, D., Martin, R., Jones, G., Paoli, J., Gée, C., 2012. How mass flow and rotational speed affect fertiliser centrifugal spreading: potential interpretation in terms of the amount of fertiliser per vane. Biosyst. Eng. 111, 133–138.
Villette, S., Piron, E., Miclet, D., 2017. Hybrid centrifugal spreading model to study the fertiliser spatial distribution and its assessment using the transverse coefficient of variation. Comput. Electron. Agric. 137, 115–129.
Virk, S.S., Mullenix, D.K., Sharda, A., Hall, J.B., Wood, C.W., Fasina, O.O., McDonald, T. P., Pate, G.L., Fulton, J.P., 2013. Case Study: Distribution uniformity of a blended fertilizer applied using a variable-rate spinner disc spreader. Appl. Eng. Agric. 29, 627–636.
Wagner, L.E., Ding, D., 1994. Representing aggregate size distributions as modified lognormal distributions. Trans. ASAE 37, 815–821.
Yildirim, Y., 2008. Technical note: effect of vane shape on fertilizer distribution uniformity in single-disc rotary fertilizer spreaders. Appl. Eng. Agric. 24, 159–163.
Yildirim, Y., 2006. Effect of cone angle and revolution speed of disc on fertilizer distribution uniformity in single-disc rotary fertilizer spreaders. J. Appl. Sci. 2875–2881.
Yule, I., 2011. The effect of fertilizer particle size on spread distribution. NZ Centre for Precision Agriculture, Massey University, Palmerston North, New Zealand, 1-9.